Nanoplastic in aqueous environments: The role of chemo-electric properties for nanoplastic-mineral interaction.

Authors:

Sascha Müller [a, b], Jacek Fiutowski [c], Maja Bar Rasmussen [b], Tonci Balic-Zunic [b], Horst-Günter Rubahn [c], Nicole R. Posth [b]

Affiliation:

[a] *Department of Biology, Microbial Ecology, Lund University.*

[b] *Department of Geosciences & Natural Resource Management, University of Copenhagen.*

[c] *Mads Clausen Institute, NanoSYD, University Southern Denmark (SDU).*

Corresponding Author:

Sascha Müller; Email: sascha.muller@biol.lu.se; Address: Department of Biology—Microbial Ecology, Sölvegatan 37, 22362 Lund, Sweden.

Keywords

Nanoplastic, Mineral, Groundwater, Adsorption

Abstract

The ever-increasing plastic production and its continuous release of primary and secondary nanoplastic particles (NP) (particles <1000µm) to the environment is an emerging contaminant for terrestrial environmental systems. Its fate and transport characteristics in the subsurface are still not fully understood, as those environments are highly complex with high mineral, chemical, biological and morphological heterogeneity. Our study focuses on the interaction between major abundant minerals occurring in the subsurface and NP under simplified water chemical conditions (1mM KCl, pH 5.5). Therefore, potential chemical effects from ions in solution can be excluded, and only the effect of mineral complexity can be assessed. Various surface-modified polystyrene nanoparticles serve as proxies for degradation (-COOH) or protein associations (-NH2) occurring in plastics in environmental settings. Here, we also compare our experimental results to DLVO double-layer force estimates. All minerals studied maintained negative charges across pH changes. Therefore, we hypothesize that adsorption behaviour is mainly “surface charge” driven (Zeta potential). Furthermore, we discuss other mechanisms, such as specific ion-binding interactions occurring in the presence of metal ions, bridging mechanisms and hydrogen bonding. Our study indicates that biogeochemical and mineralogical composition is a controlling factor in NP attachment and release processes in subsurface environments and, thus, crucial for transport in aquifers.

1. Introduction

Plastic particles follow complex transport behavior along various environmental pathways with different transport mechanisms according to their size range, solution chemistry and biogeochemical conditions. Nano-sized plastic particles (NP) (particles <1 μm) introduce additional considerations in plastic transport as their size increases the importance of particle-particle interaction and particle-collector grain interaction in the fate of plastic. Similarities between NP and engineered nanoparticles (ENP) transport exist once material-specific properties (density, aggregation behavior, hydrophobicity, surface reactivity) are accounted for (Koelmans et al. 2015). Yet, NPs differ greatly from ENPs in their particle morphology and compositional diversity. (Gigault et al. 2021). NP transport follows water cycle pathways and deposits via atmospheric precipitation, transports via surface waters (streams, sewage channels, etc.), or agricultural practices (plastic mulching), and eventually infiltrates shallow soils to reach groundwater aquifers through recharging water (Allen et al. 2019; Bergmann et al. 2019; Bläsing and Amelung 2018; Dris et al. 2015; Hurley et al. 2018; Kirstein et al. 2021; Mintenig et al. 2017; Nizzetto et al. 2016; Vollertsen 2017).

NP deposition in shallow soil is highly likely due to its complex hydrology (wetting-drying, dual porosity matrix) and biogeochemical characteristics, supporting particle retention in the shallow subsurface (Bläsing and Amelung 2018). It has been shown that pollutants and ENP infiltrate beyond shallow soils and enter the saturated zone via dominant convective transport through coarser porous media, matrix heterogeneities, well-connected macro or micropores and preferential flow paths, which develop along fractures and cracks (Kessler et al. 2012; Looms Zibar et al. 2018; Mosthaf et al. 2021). An effective filtering and physical retention process for particles is “straining” in saturated pore water. Straining is mainly a function of grain size distribution and the ratio between particle-collector grain sizes (i.e., minerals). Straining occurs until a critical ratio between the particle-collector grain size does not exceed 0.05 to 0.002 (Bradford et al. 2002; Herzig et al. 1970). As an example, if 100 nm NPs are released into saturated subsurface materials, grains in the matrix as small as 2 μm and as large as 50 μm are expected to induce straining. Groundwater aquifers, which aim to

produce a cost-effective water yield, contain hydraulic conductivity beyond the fine sand range and, therefore, in return, have grain size distributions and mean grain sizes, producing straining ratios far above the straining thresholds. Additionally, fractures or macropores in consolidated soils and aquitards may exceed those thresholds (Beven and Germann 1982). Therefore, straining becomes ineffective and leaching of nanoplastic particles <100 nm can be expected. Consequently, other mechanisms, such as the chemo-electric properties of particles and minerals at the submicron scale, become important for the transport of NPs.

Groundwater aquifer systems are foremost characterized by their complex mineral composition. As such, minerals are a major component of the subsurface aqueous environment and pose a large cumulative reactive surface. The mineral composition of an aquifer is governed by its geological evolution. Carbonates, clay minerals from the smectite, illite and kaolinite groups, quartz and other rock-forming silicates, as well as iron oxides, are among the most abundant minerals of the Earth´s crust and hence are expected as the most dominant minerals in terrestrial aquifers. Recently, molecular dynamic simulations have also shown the great potential of the hydroxyl surfaces of kaolinite to bind emerging contaminants of PFAS molecules (Loganathan and Wilson, 2022). Clay minerals and phosphate, i.e., apatite, are also known to adsorb to metal contaminants (Zhuang and Yu 2002; Li et al. 2023). Calcite and the Al- groups of feldspar effectively adsorb arsenate (As V) (Alexandratos et al. 2007; Sø et al. 2008; Yazdani et al. 2016). A surface modification of the iron-bearing silicate mineral biotite to nano FeC2O4 has also shown high removal potential for Cr(VI) and Cr(III) pollution under environmentally relevant conditions (Zeng et al. 2020). Iron oxides, in particular goethite, are known as an effective adsorbent for heavy metals and other inorganic components (i.e., fluor) or a range of organic compounds, i.e., glyphosate (Dideriksen and Stipp 2003; Liu et al. 2014; Borch et al. 2010). In addition, a wide range of studies exists on the retention capacity of different minerals and natural soils for various ENPs, such as TiO_2, ZnO_2 or AgNPs (Mustapha et al. 2020; Dong and Zhou 2020; Parsai and Kumar 2020; Coutris et al. 2012; Rahmatpour et al. 2017; Simonin et al. 2021; Torrent et al. 2019; Manik et al. 2023), to name a few. Recently, polymer-based NPs and

their effect on subsurface systems have moved into focus (i.e., Yu and Flury 2020), making NP interactions with subsurface geochemistry and mineralogy pertinent to NP fate.

Most minerals maintain a negative surface charge under environmentally relevant conditions in freshwater systems (Kosmulski 2009). A few minerals, such as iron oxides, have predominantly positive surface charges, favoring the attachment of negatively charged plastic polymers (M. Li et al. 2019). However, NP's aggregation and retain-release process strongly depend on the particle surface's physiochemical conditions and surrounding solution chemistry. (Elimelech 1994). Aggregation behaviour is often studied under batch experimental conditions, where particle size is measured over time under varying solution chemistry, and a time-resolved size increase is used to derive attachment-efficient parameters (Chen and Elimelech 2006; Alimi et al. 2022). Zhang et al. (2020) describes adsorption between NP, goethite, aluminum oxides, and kaolinite in batch-scale studies and point to the dependence of adsorption on surface charge and solution pH. However, to date a lack of studies focused on other regularly occurring minerals to address subsurface complexity remains, which we aim to address in the current study.

This study investigates whether the subsurface acts as a sink for NP due to mineral-plastic interaction alone. To this end, we i) investigate the chemo-electric properties of NP and minerals under changing solution pH conditions and ii) study adsorption behavior in batch adsorption experiments.

2. Methods:

2.1 Materials:

Non-functionalized pure polystyrene particles (PS-PLAIN) and carboxyl- functionalized polystyrene (PS-COOH) of 100 nm nominal diameter were purchased from Micromod (Micromod Partikeltechnologie GmbH, Rostock). Carboxyl-coated polystyrene is a proxy for degraded plastic, as carboxyl groups are produced at nanoplastic surfaces via ageing by UV light. (Mao et al. 2020). Amine-coated polystyrene (PS-NH2) of 100 nm nominal diameter was purchased from Sigma Aldrich and represents a proxy for the interaction of plastics with organic nitrogenous substances typically present in the subsurface. The polymers were analyzed using ATR-FTIR to confirm their chemical surface composition (**Error! Reference source not found.**). A stock solution of 1000 mg/L was prepared from the vendor's Stock suspension (10000 mg/L) for each PS type. For the experiments, a fraction of the stock was diluted with one mM Potassium chloride (KCl) to achieve the desired experimental particle concentration of 20 mg/L. The experimental PS concentrations used here are far beyond realistic environmental concentrations. Still, high concentrations were chosen to achieve mechanistic understanding and avoid the potential influence of uncertainty of analytical methods used herein at low concentrations. The three different particle coatings provide proxies for ions and physio-chemical conditions (i.e., charge) to which plastic polymers can be exposed in natural environments. Pure polymers are unlikely to occur in natural environments because producers regularly modify plastic surfaces to serve specific applications (i.e., Food, beverage, Cosmetics, etc.).

Mineral powder samples representative of the most abundant minerals in aquifers, i.e., goethite and kaolinite, were purchased from Sigma Aldrich. Quartz, feldspar, calcite, biotite and apatite samples were collected from the mineral collection at the Department of Geosciences and Natural Resource Management (IGN) at the University of Copenhagen. There, subsamples of a larger mineral were cut to access pristine, unweathered samples. The pristine sample was dry-milled for approx.10-30

min. After that, a powder suspension was made with ultra-pure Silex water. After ultra-sonication for 30 min, the mineral solution samples were wet sieved through a 20 µm mesh. After sieving, the samples were oven-dried at 30°C for 24 h. The resulting powder was stored under dark, dry conditions until further use. The mineral powders were then analyzed for major elemental and mineralogical composition using X-ray fluorescence (XRF) and X-ray diffraction (XRD), respectively (see below).

2.2 Zetapotential & Hydrodynamic radius

The Zeta potential (ZP) for polymers and minerals in 1 mM KCl was measured with the Stabino (Colloid Metrics GmbH, Germany). The Stabino instrument measures streaming potential in a 10ml PTFE chamber with an oscillating piston. The piston movement creates a mobile ion cloud around the pistons surrounding it, forming a double layer that is set in motion. This oscillating ion cloud generates voltage and is captured by two separate electrodes, which defines the streaming potential of the solution as proportional to the zeta potential of the particles. The Stabino method is advantageous for dense and polydisperse solutions as it can measure across a large particle size range (0.3 nm– 300 µm) and particle concentrations up to 40vol%. Further, the optical properties of the measurement liquid are not relevant for its measurement, unlike methods based on electrophoresis.

Mineral powders were suspended in the desired electrolyte solution (1 mM), producing a suspension of 100 mg/L for each mineral powder. To ensure full hydration of the mineral surface, the mixture was shaken with an orbital shaker for 12 h and ultra-sonicated for 30 min before measuring its Zeta potential (ZP).

The hydrodynamic radius was measured using dynamic light scattering (DLS) technology using Nano-Flex II (Colloid Metrics GmbH, Germany), which applied the heterodyne 180° backscattering principle. DLS measurements before and after the adsorption experiments add extra quantitative

and qualitative information on adsorption results when working with mineral and plastic particles. The average of the intensity (D50) is reported in the following.

2.3 Adsorption experiments

To study the adsorption behavior of NP in batch experiments, a 20 ppm NP solution was prepared by diluting a 100 ppm NP stock solution from above to the desired concentration using a one mM KCl background electrolyte. The pH of that mixture was adjusted to 5 before the experimental start using 0.05 mM HCl. The experiment was started by adding 20 mg of mineral powder to each 10 ml vial to yield a mineral concentration of 2000 ppm, which is 100 times larger than the NP concentration. There are currently no reliable measurements of NP occurrence in groundwater environments. However, as minerals define the host material of rocks, the natural abundance of minerals in groundwater logs surpasses the NP concentration by far.

Adsorption was detected spectrophotometrically using a Biotek EPOCH3 with UV cuvettes at IGN. A wavelength of 220nm was most suitable for OD (optical density) measurements (see attachment) of the different NP particles, as no interference with most minerals can be ensured. However, calcite shows OD values beyond PS-PLAIN and PS-COOH and close to PS-NH2 at 20 ppm polymer concentration. Thus, DLS provides additional evidence that clarifies contradictory (or unclear) absorbance measurement data. To develop a background signal, the suspension of NP in 1 mM KCl was analyzed before the addition of the minerals (starting concentration). After that, minerals were added, and the suspension was left for 24 hours. During those 24 hours, the vials were placed on an orbital shaker to ensure that the whole liquid was mixed in the vial. Upon conclusion of the experiment, shaking was stopped, and the experimental vials were centrifuged for 20 minutes at 3000 rpm. The supernatant was removed by decantation. The supernatant's OD at 220 nm wavelength was measured again at the final step.

The adsorption data are expressed as a percentage fraction. This fraction was calculated directly from the OD measurements because, from the calibration curves (supplement), a linear relationship

is measured between OD and particle concentration at particle concentrations below 30 ppm (**Error! Reference source not found.**). This approach is valid due to linearity below 30 ppm and has the advantage of leaving out an intermediate calculation from OD to mg/L. At concentrations >30 ppm, the OD of NP reaches saturation and takes a logarithmic shape. Consequently, interpretations of experiments beyond 30 ppm are strongly biased. Thus, 20 ppm was used herein.

2.4 Elemental and mineral composition

The mineral powders were analyzed for major elemental composition using a handheld XRF mounted in a certified portable workstation (HH-XRF, Innov-X Olympus Delta Premium 600 handheld energy-dispersive XRF spectrometer) at IGN. Powder X-ray diffraction (PXRD) analysis further checked the mineral composition using a Bruker-AXS D8 Advance diffractometer at IGN. This instrument has a Cu X-ray tube, a primary beam Ge111 monochromator (wavelength 1.54059 Å), and a silicon-strip LynxEye detector with an opening of 3.3°. The analyses were performed using the Bragg-Brentano technique with a rotating sample holder, a fixed divergence of the primary beam of 0.25°, at 2θ angles between 5-90°, in steps of 0.02° and a measuring time of 4 seconds per step for optimal statistical sample coverage. The qualitative evaluation of the sample mineral content was performed using the Bruker DIFFRAC.EVA version 7.0 software and the built-in crystallography database. The quantitative analyses were performed using the Rietveld refinement method and the Bruker DIFFRAC.TOPAS version6 software and structure files imported from the Inorganic Crystal Structure Database (ICSD,(Bergerhoff et al. 1983). The PXRD profiles were defined by fundamental parameters calibrated using a powder CeO_2 standard with an average crystallite size of 595 nm.

2.5 Imaging

After centrifugation, the solid mineral samples remaining in the vials were inspected under a He-ion microscope (Orion NanoFAB, Carl Zeiss) at the Mads Clausen Institute (MCI), University of Southern Denmark (SDU) to visualize their association with NP. The beam energy was set to 30 keV, with a

probe current ranging from 0.1 to 0.3 pA. Before imaging, no conductive coatings were applied to the samples to preserve the sample surface information. Charge compensation was ensured through a low-energy electron beam (flood gun, 433 eV) directed at the sample.

2.6 Interaction energies (DLVO)

Theoretical interaction energies were calculated based on classical DLVO using a sphere-plate relationship according to the equations provided, i.e., (Israelachvili 2011a) and (Petosa et al. 2010). Van der Waals forces (VDW) were calculated by:

$$VDW = -\frac{A_{123} * a_p}{6h(1 + \frac{h}{\lambda})}$$

Table A.1 in the supplementary section provides details on mineral- specific Hamaker constants where A_{123} is the Hamaker constant between the polymer and respective mineral in water. a_p is the particle radius, assuming 100 nm as the nominal particle diameter. *h* is the separation length between the sphere, and λ is the characteristic retardation wavelength. Retardation limits the range of the VDW forces at larger separation distances, as at larger separation distances, the polarization of dipoles is less correlated. (Henry et al. 2012).

The electric double-layer force component (EDL) was calculated as follows:

$$EDL = 64\pi\varepsilon_0\varepsilon a_p\left(\frac{k_BT}{ze}\right)^2 \tanh\left[\frac{(ze\zeta_1)}{(4k_BT)}\right]\tanh\left[\frac{(ze\zeta_2)}{(4k_BT)}\right]exp(\text{-}\kappa h)$$

With k being the Debye length estimated by:

$$\kappa = \left(\frac{2 * \mathrm{IS} * e^2 * \mathrm{NA} * 1000}{\varepsilon_0\varepsilon k_BT}\right)^{1/2}$$

Where ε_0= dielectric permittivity in vacuum (8.8541878128E-12 C^2 J^{-1} m^{-1}), $\varepsilon =$ dielectric constant in water (78.54 at 25°C), a_p= particle radius, k_B= Boltzmann constant (1.38E-23 m^2 kg s^{-2} K^{-1}), T= Temperature in Kelvin, z=ion valency of the solution, e= elementary charge constant (-1.60E-19

C),ζ_1 and ζ_2 are the Zeta potential of the polymer and mineral, respectively. IS is the ionic concentration of the solution (here 1 mM) and NA= Avogados number (6.02E+23 particles M^{-1}). Finally, the complete interaction is calculated by:

$$\mathrm{VDLVO} = \mathrm{VDW} + \mathrm{EDL}$$

given in $k_B T$ units.

3. Results & Discussion

3.1 Mineral origin and their relevance for groundwater aquifer systems

Upon entering the subsurface, NPs come into close contact with the mineral composition of the host materials. Among the hydrological characteristics (such as pore size and porosity), these mineral properties are crucial in governing the fate and transport of nanoparticles (NPs) in subsurface environments. Geological evolution defines a groundwater aquifer's mineral constituents, making the mineral composition of individual aquifers highly dependent on regional geological history. Simplifying this complex natural composition to just a few minerals is challenging. Nevertheless, a few minerals can be considered abundant in most terrestrial aquifers on a global scale due to their specific rock-forming mechanisms. Those are quartz and other rock-forming silicates, clay minerals from the smectite and kaolinite groups and illite, iron oxides such as goethite and hematite as well as carbonates. A selection of seven minerals is included in this study, and an overview of their respective aquifer abundance, as well as rock formation condition, is listed in Table 1. Among those chosen minerals, quartz, feldspar, goethite, kaolinite, and calcite are by far the most abundant.

Mineral	Geological environment (by abundance)	Formation	Aquifer type (by highest abundance)
Quartz	most rock formations, water-yielding units	As part of crust formation (e.g., crystallization in igneous rocks, crystallized from metamorphic fluids)	porous media, fractured rocks, karstic systems
Goethite	high abundance on earth in aquatic environments (lakes, soils, swamps, porous media)	Weathering product of iron-rich minerals	porous media, high-yielding aquifers
Apatite	Igneous rocks (i.e., granite), metamorphic (i.e., gneiss), sedimentary rocks as erosive-reformed products (i.e. organic marine deposits)	Crystallization in igneous rocks, precipitation in aquatic environments, metamorphic formation	porous media & fractured rocks
Biotite	Magmatic and metamorphic rocks, 2:1 phyllosilicate	Crystallization in igneous rocks, metamorphic processes	fractured igneous aquifers
Kaolinite	Type 1:1 clay low abundance in ocean sediments and a high abundance in the crust	Weathered granitic rocks	porous media and weathered soils

Feldspar	60% of Earth's crust, igneous, metamorphic	Precipitation from magma, metamorphic formation	porous media, fractured rocks
Calcite	most stable calcium carbonate mineral under atmospheric surface conditions, main constitute of limestones and marble	Precipitation in aqueous environments, diagenetic conditions.	sedimentary porous media, Karstic systems, limestone fractured aquifers

Table 1. Mineral description and their geological abundance in Earth´s environmental systems, major formation properties (Klein and Dutrow 2007), and relevance for different types of aquifer systems. As those minerals are abundant on Earth, their corresponding occurrence in all aquifer systems is given.

3.2 Mineral inspection and quality

Mineral impurities are common in natural settings. While naturally occurring impurities on minerals may dramatically alter the transport characteristics of NPs, it had to be ensured that the minerals used herein are of high quality and purity.

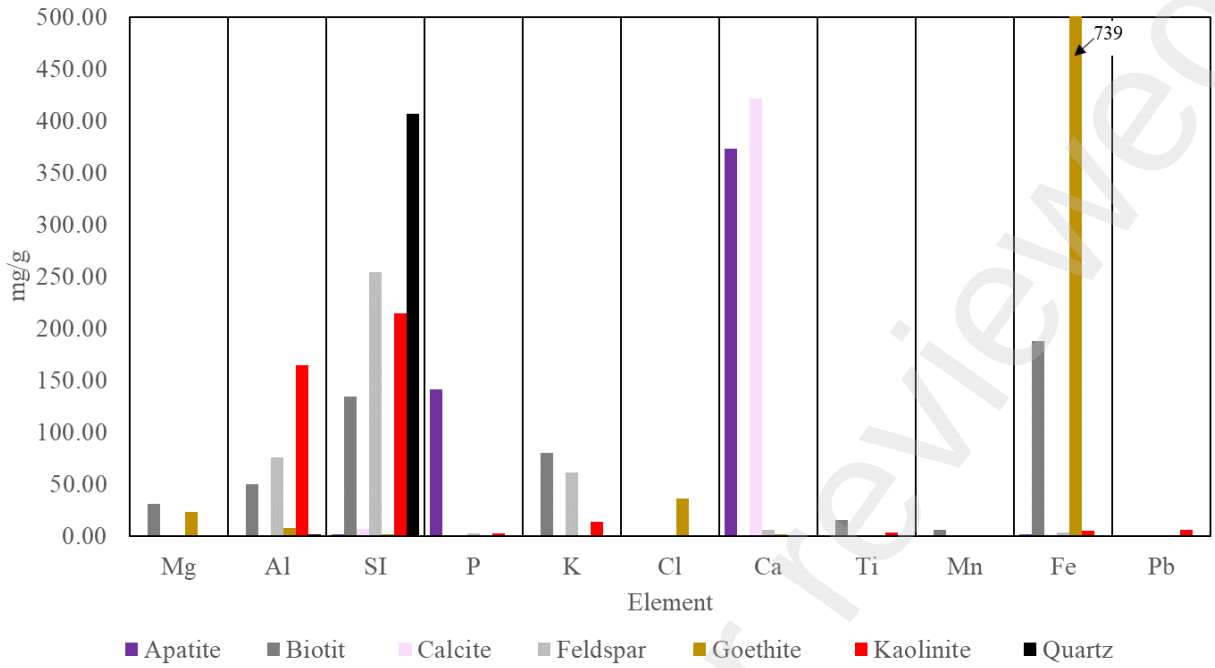

250

251 *Fig. 1. Element contents of mineral samples used (color coded) determined by XRF. Th). Small*

252 *amounts of Cl^- and Mg^{2+} in goethite are most likely a result of pre-washing of the mineral during*

253 *industrial production.*

Mineral	PXRD results
Quartz	quartz, SiO_2 (98.08%); orthoclase, $KAlSi_3O_8$ (1.92%)
Goethite	pure goethite, FeO(OH)
Apatite	hydroxylapatite, $Ca_5(PO_4)_3(OH)$, pure
Biotite	biotite, $K(Mg,Fe)_3(AlSi_3O_{10})(OH)_2$, pure
Kaolinite	kaolinite, $Al_2Si_2O_5(OH)_4$ (87.5%), quartz, SiO_2 (9.4%), plumbogummite, $PbAl_3(PO_4)(PO_3OH)(OH)_6$ (3.10%)
Feldspar	antiperthite, albite, $(KAlSi_3O_8)$ (61.9%), microcline, $(NaAlSi_3O_8)$ (38.1%),
Calcite	calcite, $CaCO_3$ (99.6%) and quartz, SiO_2 (0.4 %)

254 *Table 2. Summary of PXRD mineral compositions determined by Rietveld qualitative analysis*

255 *(using the Bruker TOPAS software). Corresponding PXRD diagrams can be found in*

256 *supplementary material. The quantitative results are expressed in wt %*

The mineral composition of the samples applied in this study is detailed in Table 2 and their chemical composition measured by XRF in Fig. 1. Apatite assembles major contents of phosphorous and calcium ions, and the XRD confirms it as hydroxylapatite. A more complex elemental composition shows biotite containing a mixture of Si, Al, Fe, Mg and K ions and its purity is confirmed by PXRD. The purity of feldspar (Al, Si, Na, K), quartz (Si) and calcite (Ca, and trace amounts of Si) is confirmed by both PXRD and XRF measurements. The latter measuring the elements with electron number greater than 11, thus not registering Na.

The kaolinite sample shows a small admixture of quartz and a mineral belonging to the plumbogummite family, which explains the small amount of Pb and P found by XRF. Small amounts of K and Fe, also detected by XRF, are normally adsorbed to kaolinite and point towards the origin of kaolinite in the zone of rock and ore metamorphism (**Error! Reference source not found.Error! Reference source not found.**). In goethite, XRF shows a distinguishable amount of Cl. This may occur when industrially produced goethite is washed clean with acid, and Cl- ions remain on the surface.

3.3 Polymer and Mineral ZP as a function of pH

In abiotic settings, the ZP of particles and minerals is considered a good indicator for deducting adsorption properties. The value for ZP is unique depending on particle surface chemistry, different ion types, and the electrolytic solution's overall ionic strength (IS) (Bhattacharjee, 2016). A 10% measurement error on the value of ZP may be expected, while potential measurement uncertainty is increased close to the iso-electric point (IEP) (Kosmulski, 2009; Nobbmann, 2017).

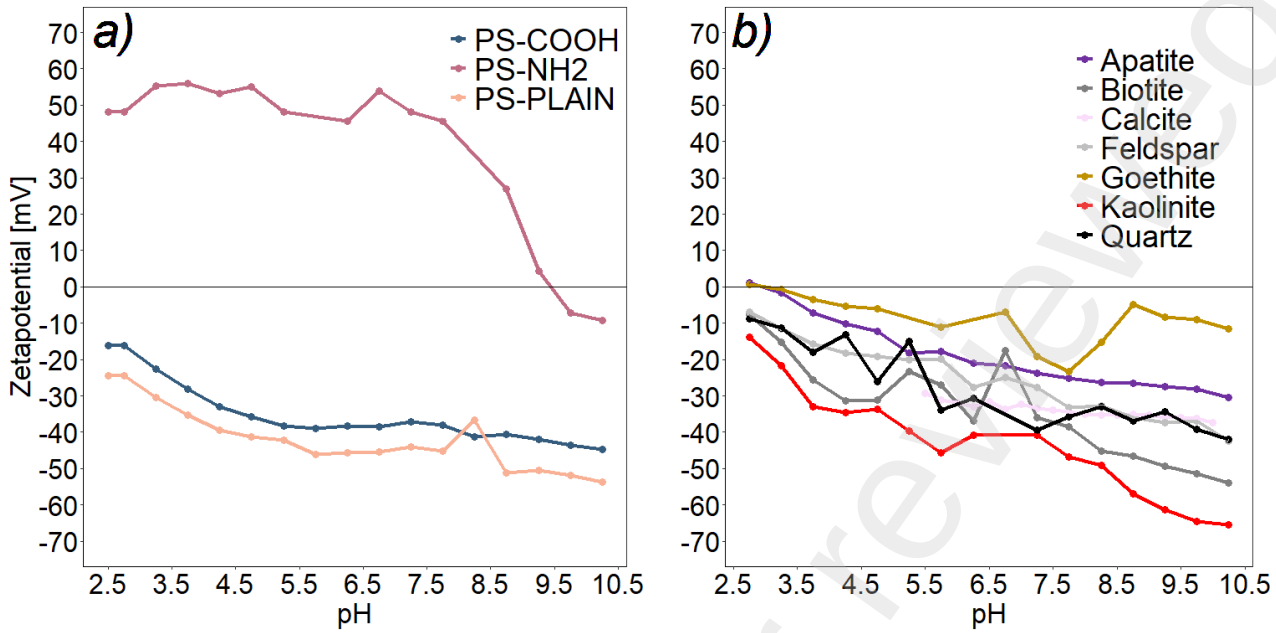

Fig. 2. ZP across pH in 1 mM KCL experimental solution. a) for non-coated Polystyrene (PS-PLAIN), for carboxylated polystyrene (PS-COOH), and amine-coated polystyrene (PS-NH2) particles and b) for minerals used in this study. Overall, the ZP decreases with decreasing pH.**Error! Reference source not found.**The ZP of polystyrene (PS) with various surface coatings and minerals is shown as a function of pH (Fig. 2). PS-PLAIN and PS-COOH particles and all minerals obtain a negative charge, contrary to the amine-coated PS, throughout a wide pH range (Fig. 2). At conditions relevant to the natural environment, i.e., pH from 4.5 to 8.5, charges vary between approximately - 40 and -10 mV, respectively, with the exception of PS-NH2 that remains positively charged. Protonation (lowering pH) or deprotonation (increasing pH) of a particle surface moves the ZP towards 0 mV with decreasing pH and vice versa when metal ions are associated at the particle surface (Kirby and Hasselbrink 2004). Protonation and deprotonation have a minor effect on the ZP of calcite, which is unstable at low pH. For calcite, charge only indirectly relates to pH as the calcite surface is dominated by CO_3^{2-} ion between pH 5 and 11 and is thus negatively charged. The surface composition is not controlled by pH but by Ca^{2+} and CO_3^{2-} availability in solution. Therefore, pH affects ZP on the surface of calcite only at constant CO_2 pressure where Ca^{2+} and pH are related (Al Mahrouqi et al. 2017).

293 The partial pressure of CO_2 was not constant during the measurements presented here. Therefore
294 calcite was unstable (dissolved), and ZP values were discarded below pH5.5.

295 For PS-NH2, the influence of OH- groups at the surface causes a reversed trend. Protonation of
296 amino groups prevails across the entire pH range. Goethite has negative ZPs across the pH range,
297 and an IEP around 8 is not reached. Goethite´s IEP may vary between pH 5- 9 (Kosmulski 2009;
298 Shrimali et al. 2016) Depending on mineral impurities. Scaratti et al. (2018) reported similar results
299 to our measurements for α-FeOOH (goethite) and attributed it to the surface-adsorbed anionic
300 species, e.g. CO_3^{2-}, SO_4^{3-} . Those anionic species are thus likely to reduce naturally occurring
301 goethite IEP far below pH 8. XRF analysis identified the presence of Cl^- ions associated with the
302 goethite used herein (Fig. 1). This indicates that the commercial goethite sample was synthesized
303 with Cl^- salts instead of NH_4^+ salts. Chloride shows a higher affinity for ion oxides and cannot
304 exchange OH- groups as easily, producing negative ZP at lower pH. (Ahmed and Maksimov 1968)
305 Therefore, the streaming potential method applied at the Stabino system captures the minor
306 presence of Cl^- ions at the surface. Different streaming potential methods directing liquid over a
307 porous sample surface, or the more general electrophoresis method based on current exciting the
308 sample may not capture such minor impurities.

309 Apatite´s ZP and IEP strongly depend on the ion type in the background solution and the type of
310 apatite and elemental impurities. Indeed, IEPs vary between pH 8 in a KNO_3 solution for
311 hydroxyapatite down to pH 6 for fluorapatite (Somasundaran and Wang 1984). A recent study
312 reported IEP as low as pH 3.5 at ten mM KCl (Zhou et al. 2020). The latter study aligns with our
313 measurements at 1 mM KCl. Apatite has the potential to release Ca^{2+} ions to the surrounding solution
314 as a function of pH, which is shown not to affect the overall electric properties of the apatite (Zhou
315 et al. 2020). Biotite and kaolinite ZPs align with measurements reported for 1 mM KCl (Filippov et al.
316 2016).

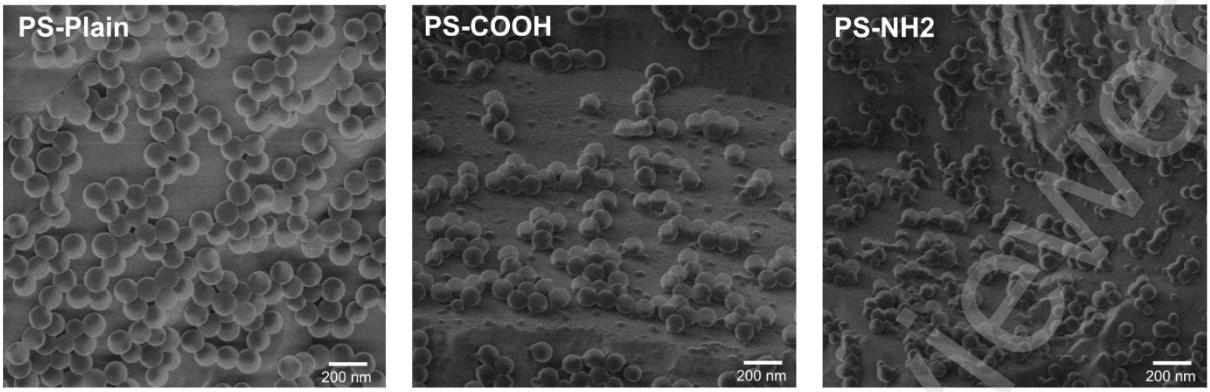

Fig. 3. HIM images of pure polymers, spherical shapes and monodisperse distribution are confirmed.

3.4 Mineral- Polymer adsorption

The interaction of NP with minerals can be interpreted from measuring NP concentrations in supernatants before and after a mineral amendment to a suspension. The results of the spectrophotometrically obtained supernatant NP concentrations expressed as a %- fraction of the original concentration are shown in Fig. 4. A value of 100 % indicated that all PS particles were absorbed to the mineral. Thus, the PS was withdrawn from the supernatant and undetected. DLS-particle sizes of the same supernatant are shown in Table 3. Using this measurement, additional information was gained on particle aggregation (size increase), destruction (size decrease), or adsorption and settling (no size detection).

Overall, DLS sizes and absorbance measurements agreed, meaning that when no adsorption was spectrophotometrically detected, the DLS size in the supernatant solution were close to the size of the original polymer (Table 3).

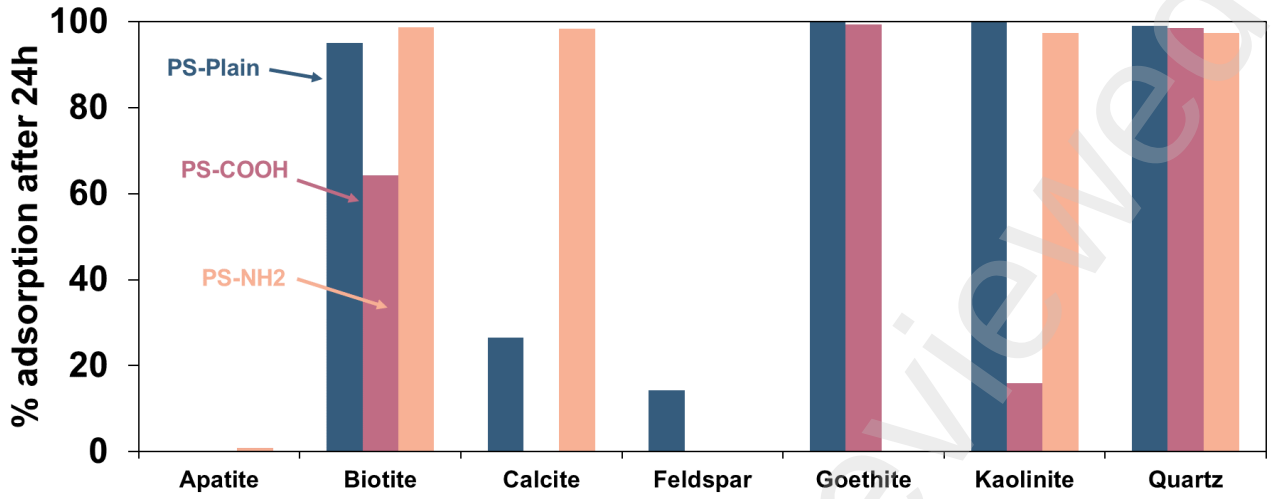

Fig. 4. Results of 24-hour adsorption experiments at pH5. Changes in NP concentrations in the supernatant are expressed in % change compared to the starting concentration. If no adsorption exists, the adsorption percentage yields 0%, while if no NPs are present, the adsorption yields 100%.

Adsorption behavior varies between mineral and NP types (Fig. 4). Often, the presence of PS particles was indicated by D50 occurring at around 100 nm, which is the original PS size. Size fractions above the background DLS- D50 of PS indicated the formation of heteroaggregates that remained in the solution after centrifugation.

	PS-PLAIN			PS-COOH			PS-NH2		
DLS-Peak	1st	2nd	3rd	1st	2nd	3rd	1st	2nd	3rd
pure particle	140.6±44			85.4±21			90.2±28.1		
Apatite	**137±42**			**87.3±16.8**			177	652	
Biotite	**150±48**			258	**65.3**		7.8	1682	
Calcite	168	>1500		**88.5±23**			5.2	648	4584
Feldpspar	**146±58**			**84.8±23**			86±26		
Goethite	592	1246	141	1396±772			298		
Kaolinite	594	1541		**85.4**	1138		2566±609		
Quartz	**183±73**			164±110			N.A.		

*Table 3. DLS sizes for pure NP in 1 mM KCl as well as the decanted solution. The measurements from the decanted solution represent a potential NP-mineral aggregate formed. If present, the 1st, 2nd, and 3rd refer to multiple peaks in the DLS signal. No adsorption is indicated if a single peak is observed screening the original particle size. Those are highlighted in **bold**. Partly adsorption is indicated when a fraction of the original particle size is measured in solution. In contrast, adsorption is indicated when only larger sizes or no observation can be made (due to gravitational particle settlement). Values highlighted in red give contradictory information compared to absorbance measurements.*

Generally, the adsorption behavior can be explained by charge-driven interactions, where oppositely charged materials attract one another. Apatite and feldspar showed potential for the lowest adsorption affinity for PS independent of their surface coating, which was expressed in an adsorption percentage close to 0%. This was confirmed by DLS for PS-NH2, where the D50 of 86nm was recorded close to the PS-NH2 original size (Table 3).

For PS-PLAIN-Kaolinite and PS-NH2-Kaolinte, effective adsorption was measured (close to 100%), while two DLS peaks at 594nm and 1541nm for the PS-PLAIN-Kaolinite solution and a single peak at 2566nm for the PS-NH2-Kaolinite solution were detected. This suggested heteroaggregation (DLS particle size increase). The lack of an absorbance signal can be attributed to the shielding of Kaolinite deposition at the PS particle surface.

A further advantage of combining DLS with absorbance measurements is shown for PS-NH2-apatite, PS-PLAIN—biotite, PS-NH2—goethite, PS-PLAIN—quartz, and PS-COOH—quartz (Table 3, red highlighted). For example, the absorbance method suggests no adsorption (close to 0%) for Apatite and PS-NH2, while a larger-sized primary and secondary DLS peak at 177nm and 652nm exists for these particles, respectively.

3.4.1 Apatite

No adsorption of PS-PLAIN and PS-COOH on the surface of apatite was observed, which was confirmed by DLS, showing the presence of a single peak close to the original polymer size. Despite the opposite charge between the apatite´s surface and the PS-NH2 as well as theoretical DLVO calculations, neither adsorption is suggested based on the absorbance measurements. However, DLS does not confirm these results. The occurrence of two major peaks, with the first peak approximately double the original polymer size and the second peak at 652nm, suggests aggregation processes have occurred. The release of Ca^{2+} ions from the apatite surface may cause homoaggregation by forming calcium amides and, hence, bridge NH2 functionalized particles (Speight et al. 2019). The visual inspection of the supernatant with HIM indicates such a process, where larger homoaggregates are shown among single particle appearances (**Error! Reference source not found.**). However, those homoaggregates do not explain a D50 of 652nm as their size in the HIM image is below that value. The HIM images also show heteroaggregates among the PS-NH2 homoaggregates. Those are approximately of the size of the D50 (**Error! Reference source not found.**). Thus, a combination of homo- and heteroaggregates can explain the second observed DLS peak. Interestingly, Zhu et al. (2003) found only a very small deposition of apatite onto NH2

surfaces at pH <7.5 using Quartz-Crystal Microbalance with Dissipation (QCMD) measurements. There, a two-stage process involving EDL interaction (pH > 7) and hydrogen bonding of NH2 head groups (NH3) (ph<7) is proposed. Unfortunately, neither the pH of the decadent solution or the elemental composition was measured to confirm such a process. Hence, the underlying mechanism can only be speculated upon, while HIM images and DLS sizes prove that aggregation occurred.

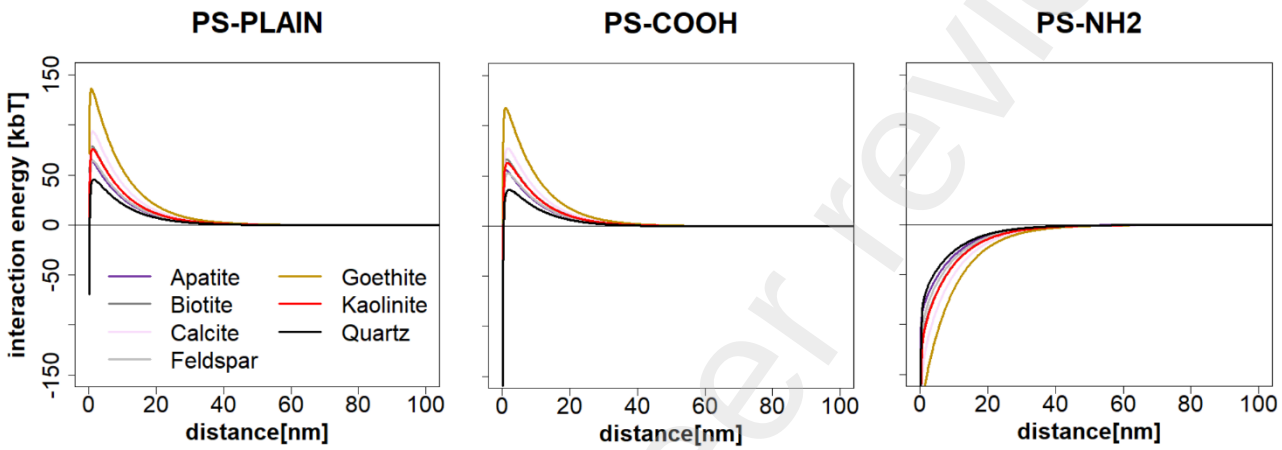

Fig. 5. Theoretical sphere-plate DLVO interaction energies at pH 5.25 in a one mM KCl solution. PS-PLAIN and PS-COOH show a strong repulsive barrier for all mineral types, while PS-NH2 shows a strong, attractive force component. DLVO can only partly reproduce adsorption observation, and it can be concluded that its predictive quality fails for more complex mineral compositions.

3.4.2 Feldspar

The adsorption results and DLS results align and show that NPs do not adsorb onto feldspar as well as reflect the original D50 particle size. From DLVO, adsorption between PS-NH2 particles and feldspar was expected (Fig. 5). Yet, the lack of adsorption between PS-NH2 and feldspar may be explained by surface free energies (Lewis-Acid base), which create a steric force component. In the presence of amino groups, feldspar increases surface hydrophobicity (Karagüzel et al. 2005), preventing the attachment of amine- coated PS. Moreover, surface adsorption onto feldspar may be influenced by the configuration of the Lewis-acid base interaction energies. The same study shows

that upon grinding, the feldspar surface mainly becomes a basal plane surface (-OH endings), where the Lewis-electron acceptor component (y_s^+) is larger than the Lewis-electron donor component (y_s). Consequently, PS-NH2 is less likely to adsorb onto the mineral surface.

3.4.3 Biotite

Based on absorbance measurements, adsorption of different magnitudes was suggested between biotite and all NP types (i.e., PS-PLAIN and PS-NH2 nearly 100%) (Fig. 4). Helium-ion microscope images also showed PS-PLAIN-biotite aggregates (Fig. 6). General DLVO calculations suggests that only adsorption of PS-NH2 on biotite is due to opposite charge interaction (Fig. 5). However, the DLS measurements show particles around the nominal diameter of PS-PLAIN in solution. The DLS of the PS-COOH groups show a primary peak at 258 nm and a secondary peak at ~65nm, which is close to the nominal diameter (Table 3). The presence of two size fractions in PS-NH2 particles is also observed (7.8nm and 1682nm). Potentially, net-negative charged biotite particles adsorb onto positive charged PS-NH2 particles, forming hetero-aggregates and thus shielding the actual polymer for the absorbance signal. This would explain the low spectrophotometric detection and the presence of a larger size fraction in the supernatant. Despite the strong repulsive barrier present (Fig. 5), biotite may still attach NP via its positive Mg+ and Al+ edges. Bray et al. 2014 show how metal release mechanisms of biotite strongly depend on the pH of the solution, while the net charge of the biotite surface is unaffected. More specifically, they show that around pH 5 (experimental pH used herein), biotite contains only low amounts of Mg2+, while Al+ remains exposed on the edges. Additionally., it is shown that biotite grain edges exceed the reactivity of the basal planes between 71-131 times (Hodson 2006). Hence, PS-PLAIN may adsorb onto the positively charged edges of the biotite mineral. A slightly modified mechanism can explain the observed adsorption for PS-COOH NPs. Here, divalent positive Mg2+ ions bridge the COOH groups at the polymer surface and cause adsorption. This mechanism is well known for organic matter in the presence of COOH groups (Adusei-Gyamfi et al. 2019). But it is less effective for Mg2+ due to the affinity for Mg to water, where

426 COOH groups cannot dehydrate Mg effectively (Carter-Fenk et al. 2021) yielding less effective
427 bridging.

428 *3.4.4 Calcite*

429 From the absorbance measurements, calcite- PS interaction was considered charge driven, as
430 similar charged PS-PLAIN and PS-COOH remained in solution, while PS-NH2 particles were fully
431 absorbed. This process was largely confirmed from the DLS measurements, where the original
432 sizes of the plain and COOH polymers are still in solution. The PS-NH2 sample shows three
433 peaks, with the largest occurring at 648 nm and a second even larger peak at 4588 nm. This
434 suggests the occurrence of aggregation processes. HIM inspection does not show clear PS-NH2-
435 calcite aggregates formations, but rather points towards homoaggregation of PS-NH2 (**Error!**
436 **Reference source not found.**). The presence of divalent ions Ca^{2+} in solution can be an effective
437 coagulant if the concentration is close to the critical coagulation concentration (CCC). This
438 suggests that calcite is dissolved and the release of Ca^{2+} into solution provoked homoaggregation
439 of the particles causing a large range of DLS sizes.

440 3.4.5 Kaolinite

441 The 1:1 clay kaolinite effectively adsorbs PS-PLAIN and PS-NH2, while it does not effectively adsorb
442 PS-COOH. The adsorption behavior for PS-NH2 is predicted with DLVO (Fig. 5) as well as confirmed
443 by DLS measurements (Table 3). In contrast, PS-PLAIN and PS-COOH show modified adsorption.
444 Kaolinite has a high charge heterogeneity with net-negative charge but carries positively charged
445 Al+ ions on the edges, which, depending on pH and IS, initiates aggregation processes. The
446 increasing role of positive charge groups at the kaolinite surface is shown at pH below 6- 6.5 and at
447 IS of 1 mM NaCl (Tombácz and Szekeres 2006). While ZP under current study conditions of pH 5.5
448 is net negative (Fig. 2), positive chargers are present. Consequently, PS-PLAIN particles without
449 any surfactant will be attracted to the positive sites and thus get adsorbed to the kaolinite matrix, that
450 is also expressed in the DLS primary sizes of 594nm. DLVO calculations cannot confirm that
451 process, as it does not account for charge heterogeneities. Adsorption to kaolinite is low to PS-

COOH likely due to the strong steric force component introduced by the -COOH groups on the polymer. Those stabilize the polymer against aggregation, which is also confirmed by the DLS measurements.

3.4.6 Goethite

Goethite showed a high affinity for negatively charged particles of PS-PLAIN and PS-COOH, while no adsorption to the PS-NH2 particles occurred. From the DLS measurements, a larger fraction was still present in the PS-PLAIN and PS-COOH of 592nm and 1396, respectively. This suggests either homoaggregates or heteroaggregates between iron hydroxyl-oxide and polymers. No absorbance is detected at the wavelength of 220nm from the absorbance spectra of goethite (**Error! Reference source not found.**). This suggests that goethite or an iron species coats the polymer surface and shields it when absorbance is measured. Hence, no absorbance at 220nm was detected. Based on our ZP measurements and the consequent DLVO calculations, such interactions are not suggested (as discussed above). Nonetheless, it is commonly observed that attractive electrostatic interactions between iron oxides and negatively charged polymers occur (i.e., Alimi et al. 2018; Zhang et al. 2020). The visualization of such hetero-aggregates confirms the adsorption between the PS-PLAIN and goethite (Fig. 6A and **Error! Reference source not found.**). No adsorption occurred between goethite and PS-NH2 due to similar charges for the two phases. Nonetheless, DLS measurements of the PS-NH2- goethite supernatant show a peak at 298nm (Table 3) and HIM imaging shows clearly homoaggregates (**Error! Reference source not found.**), evidently pointing towards homoaggregate not adsorbed to the mineral phase. Different mechanisms may cause the release of iron from goethite in the presence of organic molecules. Particularly at lower pH <8, the release of Fe(III) species from the surface is common (Li et al. 2022). Those may attach to the surface of the PS-NH2 particles and cause a partial aggregation, which the DLS detects (Table 3) and HIM imaging confirms (**Error! Reference source not found.**).

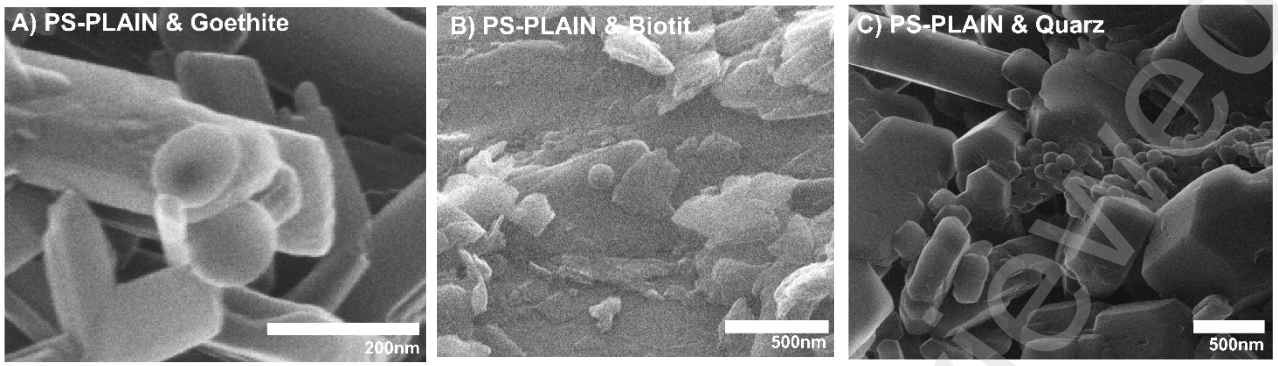

Fig. 6. HIM image of the mineral-plastic interface in the pellet.

3.4.7 Quartz

Quartz showed effective adsorption to all NPs despite the similarly charged surfaces of PS-PLAIN and PS-COOH, while this was expected only for PS-NH2 according to the DLVO. The measured DLS sizes show a small size increase of the PS-PLAIN and PS-COOH supernatant, while no signal was detected for the PS-NH2 supernatant. The latter evidently pointed towards an effective adsorption of PS-NH2 and was confirmed by HIM images (**Error! Reference source not found.**A). Furthermore, the HIM images of the pellet and supernatant for PS-PLAIN and PS-COOH with quartz can explain the observed discrepancy between absorbance - and DLS measurements. Adsorption of PS-Plain to the quartz pellet is indicated by HIM images (Fig. 6). HIM imaging did not detect PS-PLAIN and PS-COOH NPs in the supernatant (**Error! Reference source not found.**B and C), but quartz particles below 1 µm were visible. Thus, the DLS sizes of 183 nm and 164 nm for the PS-PLAIN and PS-COOH supernatants are misleading and reflect suspended quartz particles, not NPs.

The attraction between PS-PLAIN and PS-COOH as exemplified in Fig. 6, can be explained by the small amount of orthoclase measured by PXRD (Table 2). Orthoclase has Al^{3+} sides, with local positive charges, which create attractive adsorption conditions for PS-PLAIN and PS-COOH.

Alternative processes can take place at the quartz surface which can explain such unexpected adsorption behavior. Breaking Si-O bonds upon grinding, the oxide surface becomes unsaturated

and in contact with water becomes hydroxylated which changes its surface physiochemical properties. When PS and particular PS-COOH are present in that water, the polymers OH^- ending may absorb the unsaturated endings (Zheng et al. 2024). However, such a process is speculative and may be interfered with by water molecules, creating a hydration layer on the quartz surface (non-DLVO force "solvation") and thus creating a near-surface repulsive energy barrier. To investigate such a process, a different study with a different hypothesis needs to be set up.

The interactions between different functionalized NPs and the minerals evaluated in this manuscript is presented in a conceptual manner to display the processes described in this study in Fig. 7.

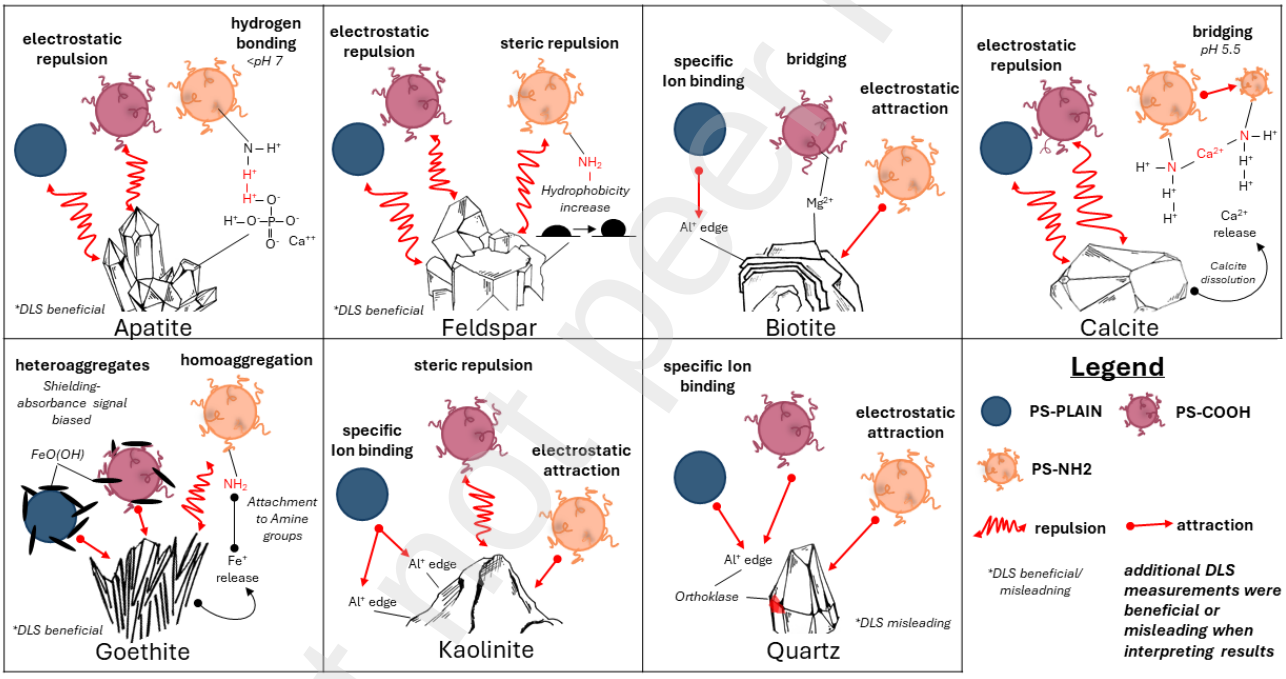

Fig. 7. Conceptual summary of adsorption results of different functionalized nanoplastic with various minerals. If not otherwise stated, electrostatic interaction was not dominant, and other processes may be more relevant. Additional DLS measurements of the supernatant were beneficial for indicated minerals to explore mechanisms between NPs and minerals.

4. Implications and Conclusion

Nanoparticles released into the aquatic environment interact with minerals in the subsurface environment. Here, we study the interaction of different surface-modified polystyrene nanospheres with the most abundant mineral species in terrestrial freshwater environments. The interaction is explored using batch adsorption experiments in combination with DLS measurements, visual inspection using HIM and compared with theoretical DLVO calculations. We show that mineral-specific interactions with PS particles exist. The interaction is largely charge-driven as DLVO theory overall aligns well with the observation. However, theoretical calculations fail to predict interactions when a more complex mineralogical structure is present and specific ion binding and bridging processes dominate the interaction.

Main findings include:

- Zeta potential varies greatly with pH for minerals and nanoplastics, while under environmentally relevant pH conditions (pH 4.5-8), stronger negative charges are predominant for both minerals and PS
- The interaction between minerals and plastic is mainly charge-driven, where Zeta potential is a good indicator of their interaction behavior
- Clay minerals may not be efficient in removing NP particles from the liquid phase under environmentally relevant pH conditions
- More complex interaction is often associated with $-NH_2$ groups at the polymer surface
- Bridging interaction occurs when Ca-containing minerals are present, minerals with Al- edges or Fe- release drive specific ion binding interaction, and Phosphor induces hydrogen bonding mechanisms

Our findings highlight implications for the fate and transport processes of nanoplastic in terrestrial freshwater environments. The mineral interaction with nanoplastic particles impacts nutrient-rich interfaces at the hyporheic zone or wetlands, groundwater discharge zones in agriculturally impacted

streams or lakes, redox boundaries in the aquifer, recharge areas near coastal saltwater wedges, and wastewater treatment plants.

In future studies, mineral-plastic interaction should be studied more systematically regarding aquifer and groundwater-related systems' biogeochemical and mineral complexity. This study indicates that biogeochemical and mineralogical composition controls the attachment and release of NP in porewaters, and therefore determining its transport in aquifers.

Acknowledgements

This research was financially supported by the Villum Foundation (grant 00022942); The microscopy imaging was supported by Interreg 6a Deutschland-Denmark Program project PlastTrack (grant number 07-1-22 1). JF and HGR are supported by UFM5229-0001B, project NANOCHEM, National Infrastructure. NP was supported by the VILLUM FONDEN (grant 15397) and the Carlsberg Foundation (grant CFF22-0963) to N.R.P.

References

Abbot, Steven, and Nigel Holmes. 2013. *Nanocoatings: Principles and Practice*. Lancester, Pennsylvania,USA: DEStech Publications, Inc.

Adusei-Gyamfi, Junias, Baghdad Ouddane, Luuk Rietveld, Jean-Paul Cornard, and Justine Criquet. 2019. “Natural Organic Matter-Cations Complexation and Its Impact on Water Treatment: A Critical Review.” *Water Research* 160 (September):130–47. https://doi.org/10.1016/j.watres.2019.05.064.

Ahmed, S., and D. Maksimov. 1968. “Studies of the Oxide Surfaces at the Liquid–Solid Interface. Part II. Fe Oxides.” *Canadian Journal of Chemistry* 46.

Al Mahrouqi, Dawoud, Jan Vinogradov, and Matthew D. Jackson. 2017. “Zeta Potential of Artificial and Natural Calcite in Aqueous Solution.” *Advances in Colloid and Interface Science* 240 (February):60–76. https://doi.org/10.1016/j.cis.2016.12.006.

Alexandratos, Vasso G., Evert J. Elzinga, and Richard J. Reeder. 2007. “Arsenate Uptake by Calcite: Macroscopic and Spectroscopic Characterization of Adsorption and Incorporation Mechanisms.” *Geochimica et Cosmochimica Acta* 71 (17): 4172–87. https://doi.org/10.1016/j.gca.2007.06.055.

Alimi, Olubukola S., Jeffrey Farner Budarz, Laura M. Hernandez, and Nathalie Tufenkji. 2018. “Microplastics and Nanoplastics in Aquatic Environments: Aggregation, Deposition, and Enhanced Contaminant Transport.” *Environmental Science & Technology* 52 (4): 1704–24. https://doi.org/10.1021/acs.est.7b05559.

Alimi, Olubukola S., Jeffrey M. Farner, Laura Rowenczyk, Adamo R. Petosa, Dominique Claveau-Mallet, Laura M. Hernandez, Kevin J. Wilkinson, and Nathalie Tufenkji. 2022. “Mechanistic Understanding of the Aggregation Kinetics of Nanoplastics in Marine Environments: Comparing Synthetic and Natural Water Matrices.” *Journal of Hazardous Materials Advances* 7 (August):100115. https://doi.org/10.1016/j.hazadv.2022.100115.

Allen, Steve, Deonie Allen, Vernon R. Phoenix, Gaël Le Roux, Pilar Durántez Jiménez, Anaëlle Simonneau, Stéphane Binet, and Didier Galop. 2019. “Atmospheric Transport and Deposition of Microplastics in a Remote Mountain Catchment.” *Nature Geoscience* 12 (5): 339–44. https://doi.org/10.1038/s41561-019-0335-5.

Bergerhoff, G., R. Hundt, R. Sievers, and I. D. Brown. 1983. “The Inorganic Crystal Structure Data Base.” *Journal of Chemical Information and Computer Sciences* 23 (2): 66–69. https://doi.org/10.1021/ci00038a003.

Bergmann, Melanie, Sophia Mützel, Sebastian Primpke, Mine B. Tekman, Jürg Trachsel, and Gunnar Gerdts. 2019. “White and Wonderful? Microplastics Prevail in Snow from the Alps to the Arctic.” *Science Advances* 5 (8): eaax1157. https://doi.org/10.1126/sciadv.aax1157.

Beven, Keith, and Peter Germann. 1982. “Macropores and Water Flow in Soils.” *Water Resources Research* 18 (5): 1311–25. https://doi.org/10.1029/WR018i005p01311.

Bläsing, Melanie, and Wulf Amelung. 2018. “Plastics in Soil: Analytical Methods and Possible Sources.” *Science of The Total Environment* 612 (January):422–35. https://doi.org/10.1016/j.scitotenv.2017.08.086.

Borch, Thomas, Ruben Kretzschmar, Andreas Kappler, Philippe Van Cappellen, Matthew Ginder-Vogel, Andreas Voegelin, and Kate Campbell. 2010. “Biogeochemical Redox Processes and Their Impact on Contaminant Dynamics.” *Environmental Science & Technology* 44 (1): 15–23. https://doi.org/10.1021/es9026248.

Bradford, Scott A., Scott R. Yates, Mehdi Bettahar, and Jirka Simunek. 2002. “Physical Factors Affecting the Transport and Fate of Colloids in Saturated Porous Media: FACTORS AFFECTING THE FATE OF COLLOIDS.” *Water Resources Research* 38 (12): 63-1-63–12. https://doi.org/10.1029/2002WR001340.

Bray, Andrew W., Liane G. Benning, Steeve Bonneville, and Eric H. Oelkers. 2014. “Biotite Surface Chemistry as a Function of Aqueous Fluid Composition.” *Geochimica et Cosmochimica Acta* 128 (March):58–70. https://doi.org/10.1016/j.gca.2013.12.002.

Carter-Fenk, Kimberly A., Abigail C. Dommer, Michelle E. Fiamingo, Jeongin Kim, Rommie E. Amaro, and Heather C. Allen. 2021. “Calcium Bridging Drives Polysaccharide Co-Adsorption to a Proxy Sea Surface Microlayer.” *Physical Chemistry Chemical Physics* 23 (30): 16401–16. https://doi.org/10.1039/D1CP01407B.

Chen, Kai Loon, and Menachem Elimelech. 2006. “Aggregation and Deposition Kinetics of Fullerene (C_{60}) Nanoparticles.” *Langmuir* 22 (26): 10994–1. https://doi.org/10.1021/la062072v.

Coutris, Claire, Erik Jautris Joner, and Deborah Helen Oughton. 2012. “Aging and Soil Organic Matter Content Affect the Fate of Silver Nanoparticles in Soil.” *Science of The Total Environment* 420 (March):327–33. https://doi.org/10.1016/j.scitotenv.2012.01.027.

Dideriksen, K., and S.L.S. Stipp. 2003. “The Adsorption of Glyphosate and Phosphate to Goethite: A Molecular-Scale Atomic Force Microscopy Study.” *Geochimica et Cosmochimica Acta* 67 (18): 3313–27. https://doi.org/10.1016/S0016-7037(02)01369-8.

Dong, Feng, and Yan Zhou. 2020. “Distinct Mechanisms in the Heteroaggregation of Silver Nanoparticles with Mineral and Microbial Colloids.” *Water Research* 170 (March):115332. https://doi.org/10.1016/j.watres.2019.115332.

Dris, Rachid, Johnny Gasperi, Vincent Rocher, Mohamed Saad, Nicolas Renault, and Bruno Tassin. 2015. “Microplastic Contamination in an Urban Area: A Case Study in Greater Paris.” *Environmental Chemistry* 12 (5): 592. https://doi.org/10.1071/EN14167.

Elimelech, Menachem. 1994. “Particle Deposition on Ideal Collectors from Dilute Flowing Suspensions: Mathematical Formulation, Numerical Solution, and Simulations.” *Separations Technology* 4 (4): 186–212. https://doi.org/10.1016/0956-9618(94)80024-3.

Filby, André. 2009. “Interaction of Colloids with Mineral Surfaces: A Microscopical and Nanoscopical Approach.” DISSERTATION, Karlsruhe: Universität Fridericiana zu Karlsruhe.

Filippov, L.O., Q. Dehaine, and I.V. Filippova. 2016. “Rare Earths (La, Ce, Nd) and Rare Metals (Sn, Nb, W) as by-Products of Kaolin Production – Part 3: Processing of Fines Using Gravity and Flotation.” *Minerals Engineering* 95 (September):96–106. https://doi.org/10.1016/j.mineng.2016.06.004.

Gigault, Julien, Hind El Hadri, Brian Nguyen, Bruno Grassl, Laura Rowenczyk, Nathalie Tufenkji, Siyuan Feng, and Mark Wiesner. 2021. “Nanoplastics Are Neither Microplastics nor Engineered Nanoparticles.” *Nature Nanotechnology*, April. https://doi.org/10.1038/s41565-021-00886-4.

Henry, Christophe, Jean-Pierre Minier, and Grégory Lefèvre. 2012. “Towards a Description of Particulate Fouling: From Single Particle Deposition to Clogging.” *Advances in Colloid and Interface Science* 185–186 (December):34–76. https://doi.org/10.1016/j.cis.2012.10.001.

Herzig, J. P., D. M. Leclerc, and P. Le. Goff. 1970. “Flow of Suspensions through Porous Media—Application to Deep Filtration.” *Industrial & Engineering Chemistry* 62 (5): 8–35. https://doi.org/10.1021/ie50725a003.

Hodson, Mark E. 2006. “Does Reactive Surface Area Depend on Grain Size? Results from PH 3, 25°C Far-from-Equilibrium Flow-through Dissolution Experiments on Anorthite and Biotite.” *Geochimica et Cosmochimica Acta* 70 (7): 1655–67. https://doi.org/10.1016/j.gca.2006.01.001.

Hurley, Rachel, Jamie Woodward, and James J. Rothwell. 2018. “Microplastic Contamination of River Beds Significantly Reduced by Catchment-Wide Flooding.” *Nature Geoscience* 11 (4): 251–57. https://doi.org/10.1038/s41561-018-0080-1.

Israelachvili, Jacob N. 2011a. “Electrostatic Forces between Surfaces in Liquids.” In *Intermolecular and Surface Forces*, 291–340. Elsevier. https://doi.org/10.1016/B978-0-12-375182-9.10014-4.

———. 2011b. *Intermolecular and Surface Forces*. Elsevier. https://doi.org/10.1016/C2009-0-21560-1.

Karagüzel, C., M.F. Can, E. Sönmez, and M.S. Çelik. 2005. “Effect of Electrolyte on Surface Free Energy Components of Feldspar Minerals Using Thin-Layer Wicking Method.” *Journal of Colloid and Interface Science* 285 (1): 192–200. https://doi.org/10.1016/j.jcis.2004.11.018.

Kessler, T.C., K.E.S. Klint, B. Nilsson, and P.L. Bjerg. 2012. “Characterization of Sand Lenses Embedded in Tills.” *Quaternary Science Reviews* 53 (October):55–71. https://doi.org/10.1016/j.quascirev.2012.08.011.

Kirby, Brian J., and Ernest F. Hasselbrink. 2004. “Zeta Potential of Microfluidic Substrates: 1. Theory, Experimental Techniques, and Effects on Separations.” *ELECTROPHORESIS* 25 (2): 187–202. https://doi.org/10.1002/elps.200305754.

Kirstein, Inga V., Fides Hensel, Alessio Gomiero, Lucian Iordachescu, Alvise Vianello, Hans B. Wittgren, and Jes Vollertsen. 2021. “Drinking Plastics? – Quantification and Qualification of Microplastics in Drinking Water Distribution Systems by MFTIR and Py-GCMS.” *Water Research* 188 (January):116519. https://doi.org/10.1016/j.watres.2020.116519.

Klein, Cornelis, and Barbara Dutrow. 2007. *Manual of Mineral Science*. John Wiley & Sons. https://www.wiley.com/en-us/Manual+of+Mineral+Science%2C+23rd+Edition-p-9781119111696R150.

Koelmans, Albert A., Ellen Besseling, and Won J. Shim. 2015. “Nanoplastics in the Aquatic Environment. Critical Review.” In *Marine Anthropogenic Litter*, edited by Melanie Bergmann, Lars Gutow, and Michael Klages, 325–40. Cham: Springer International Publishing. https://doi.org/10.1007/978-3-319-16510-3_12.

Kosmulski, Marek. 2009. *Surface Charging and Points of Zero Charge*. CRC Press.

Li, Ji, Chenlu Shi, Wenbin Zeng, Yaru Wang, Zebin Hong, Yibing Ma, and Liping Fang. 2022. “Distinct Roles of PH and Organic Ligands in the Dissolution of Goethite by Cysteine.” *Journal of Environmental Sciences* 113 (March):260–68. https://doi.org/10.1016/j.jes.2021.06.011.

Li, Meng, Lei He, Mengya Zhang, Xianwei Liu, Meiping Tong, and Hyunjung Kim. 2019. “Cotransport and Deposition of Iron Oxides with Different-Sized Plastic Particles in Saturated Quartz Sand.” *Environmental Science & Technology* 53 (7): 3547–57. https://doi.org/10.1021/acs.est.8b06904.

Li, Zhiliang, Yi Qiu, Dongye Zhao, Jian Li, Guanlin Li, Hui Jia, Daolin Du, et al. 2023. “Application of Apatite Particles for Remediation of Contaminated Soil and Groundwater: A Review and Perspectives.” *Science of The Total Environment* 904 (December):166918. https://doi.org/10.1016/j.scitotenv.2023.166918.

Liu, Haibo, Tianhu Chen, and Ray L. Frost. 2014. “An Overview of the Role of Goethite Surfaces in the Environment.” *Chemosphere* 103 (May):1–11. https://doi.org/10.1016/j.chemosphere.2013.11.065.

Loganathan, Narasimhan, and Angela K. Wilson. 2022. “Adsorption, Structure, and Dynamics of Short- and Long-Chain PFAS Molecules in Kaolinite: Molecular-Level Insights.” *Environmental Science & Technology* 56 (12): 8043–52. https://doi.org/10.1021/acs.est.2c01054.

Looms Zibar, Majken Caroline, Anja Klotzsche, Jan van der Kruk, Thomas Hauerberg Larsen, Anders Edsen, Nina Tuxen, Nancy Hamburger, Johanna Keskinen, and Lars Nielsen. 2018. “Mapping Sand Layers in Clayey till Using Crosshole Ground-Penetrating Radar.” *GEOPHYSICS* 83 (1): A21–26. https://doi.org/10.1190/geo2017-0297.1.

Manik, Rima, Mahima John Horta, and Seetha N. 2023. “Fate and Transport of Engineered Nanoparticles in the Subsurface: Current Understanding, Challenges, and Future Scope.” In *Emerging Aquatic Contaminants*, 129–72. Elsevier. https://doi.org/10.1016/B978-0-323-96002-1.00012-2.

Mao, Yufeng, Hong Li, Xiaoliu Huangfu, Yao Liu, and Qiang He. 2020. “Nanoplastics Display Strong Stability in Aqueous Environments: Insights from Aggregation Behaviour and Theoretical Calculations.” *Environmental Pollution* 258 (March):113760. https://doi.org/10.1016/j.envpol.2019.113760.

Mintenig, S. M., I. Int-Veen, M. G. J. Löder, S. Primpke, and G. Gerdts. 2017. “Identification of Microplastic in Effluents of Waste Water Treatment Plants Using Focal Plane Array-Based Micro-Fourier-Transform Infrared Imaging.” *Water Research* 108 (January):365–72. https://doi.org/10.1016/j.watres.2016.11.015.

Mosthaf, K., M. Rolle, U. Petursdottir, J. Aamand, and P. R. Jørgensen. 2021. “Transport of Tracers and Pesticides Through Fractured Clayey Till: Large Undisturbed Column Experiments and Model-Based Interpretation.” *Water Resources Research* 57 (5). https://doi.org/10.1029/2020WR028019.

Mustapha, S., M. M. Ndamitso, A. S. Abdulkareem, J. O. Tijani, D. T. Shuaib, A. O. Ajala, and A. K. Mohammed. 2020. “Application of TiO2 and ZnO Nanoparticles Immobilized on Clay in Wastewater Treatment: A Review.” *Applied Water Science* 10 (1): 49. https://doi.org/10.1007/s13201-019-1138-y.

Nizzetto, Luca, Gianbattista Bussi, Martyn N. Futter, Dan Butterfield, and Paul G. Whitehead. 2016. “A Theoretical Assessment of Microplastic Transport in River Catchments and Their Retention by Soils and River Sediments.” *Environmental Science: Processes & Impacts* 18 (8): 1050–59. https://doi.org/10.1039/C6EM00206D.

Nobbmann, Ulf. 2017. “Zetasizer: What Is the Zeta Potential Deviation?” Malvern Panalytical. Zetasizer: What Is the Zeta Potential Deviation? May 9, 2017. https://www.materials-talks.com/blog/2017/09/05/what-is-the-zeta-deviation/.

Novich, B. E., and T. A. Ring. 1984. “Colloid Stability of Clays Using Photon Correlation Spectroscopy.” *Clays and Clay Minerals* 32 (5): 400–406. https://doi.org/10.1346/CCMN.1984.0320508.

Oliveira Baldoino, Rogerio de, Marisa Bezerra deMelloMonte, Elaynne RohemPeçanha, and Laurindo deSallesLealFilho. 2017. “Fundamental Aspects from Bayóvar Phosphate Ore Concentration.” In . Cape Town, South Africa.

Parsai, Tanushree, and Arun Kumar. 2020. “Stability and Characterization of Mixture of Three Particle System Containing ZnO-CuO Nanoparticles and Clay.” *Science of The Total Environment* 740 (October):140095. https://doi.org/10.1016/j.scitotenv.2020.140095.

Petosa, Adamo R., Deb P. Jaisi, Ivan R. Quevedo, Menachem Elimelech, and Nathalie Tufenkji. 2010. “Aggregation and Deposition of Engineered Nanomaterials in Aquatic Environments: Role of Physicochemical Interactions.” *Environmental Science & Technology* 44 (17): 6532–49. https://doi.org/10.1021/es100598h.

Rahmatpour, Samaneh, Mehran Shirvani, Mohammad R. Mosaddeghi, and Mehdi Bazarganipour. 2017. “Retention of Silver Nano-Particles and Silver Ions in Calcareous Soils: Influence of Soil Properties.” *Journal of Environmental Management* 193 (May):136–45. https://doi.org/10.1016/j.jenvman.2017.01.062.

Scaratti, Gidiane, Thalita Grando Rauen, Vanessa Zanon Baldissarelli, Humberto Jorge José, and Regina De Fátima Peralta Muniz Moreira. 2018. “Residue-Based Iron Oxide Catalyst for the Degradation of Simulated Petrochemical Wastewater via Heterogeneous Photo-Fenton Process.” *Environmental Technology* 39 (20): 2559–67. https://doi.org/10.1080/09593330.2017.1361474.

Shrimali, Kaustubh, Jiaqi Jin, Behzad Vaziri Hassas, Xuming Wang, and Jan D. Miller. 2016. “The Surface State of Hematite and Its Wetting Characteristics.” *Journal of Colloid and Interface Science* 477 (September):16–24. https://doi.org/10.1016/j.jcis.2016.05.030.

Simonin, Marie, Jean M.F. Martins, Gaëlle Uzu, Lorenzo Spadini, Aline Navel, and Agnès Richaume. 2021. “Low Mobility of CuO and TiO2 Nanoparticles in Agricultural Soils of Contrasting Texture and Organic Matter Content.” *Science of The Total Environment* 783 (August):146952. https://doi.org/10.1016/j.scitotenv.2021.146952.

Sø, Helle U., Dieke Postma, Rasmus Jakobsen, and Flemming Larsen. 2008. “Sorption and Desorption of Arsenate and Arsenite on Calcite.” *Geochimica et Cosmochimica Acta* 72 (24): 5871–84. https://doi.org/10.1016/j.gca.2008.09.023.

Somasundaran, P., and Y. H. C. Wang. 1984. “Surface Chemical Characteristics and Adsorption Properties of Apatite.” In *Adsorption on and Surface Chemistry of Hydroxyapatite*, edited by

753 Dwarika N. Misra, 129–49. Boston, MA: Springer US. https://doi.org/10.1007/978-1-4757-
754 9012-2_9.
755 Speight, Isaiah R., Stephen C. Chmely, Timothy P. Hanusa, and Arnold L. Rheingold. 2019.
756 “Mechanochemically Directed Metathesis in Group 2 Chemistry: Calcium Amide Formation
757 without Solvent.” *Chemical Communications* 55 (15): 2202–5.
758 https://doi.org/10.1039/C8CC10155H.
759 Tombácz, Etelka, and Márta Szekeres. 2006. “Surface Charge Heterogeneity of Kaolinite in
760 Aqueous Suspension in Comparison with Montmorillonite.” *Applied Clay Science* 34 (1–4):
761 105–24. https://doi.org/10.1016/j.clay.2006.05.009.
762 Torrent, Laura, Eva Marguí, Ignasi Queralt, Manuela Hidalgo, and Mònica Iglesias. 2019.
763 “Interaction of Silver Nanoparticles with Mediterranean Agricultural Soils: Lab-Controlled
764 Adsorption and Desorption Studies.” *Journal of Environmental Sciences* 83
765 (September):205–16. https://doi.org/10.1016/j.jes.2019.03.018.
766 Vollertsen. 2017. *Microplastic in Danish Wastewater Sources, Occurrences and Fate*. 1906.
767 Danish Environmental Protection Agency.
768 Xu, Chen-yang, Kai-ying Deng, Jiu-yu Li, and Ren-kou Xu. 2015. “Impact of Environmental
769 Conditions on Aggregation Kinetics of Hematite and Goethite Nanoparticles.” *Journal of*
770 *Nanoparticle Research* 17 (10): 394. https://doi.org/10.1007/s11051-015-3198-8.
771 Yazdani, Maryam (Roza), Tanja Tuutijärvi, Amit Bhatnagar, and Riku Vahala. 2016. “Adsorptive
772 Removal of Arsenic(V) from Aqueous Phase by Feldspars: Kinetics, Mechanism, and
773 Thermodynamic Aspects of Adsorption.” *Journal of Molecular Liquids* 214 (February):149–
774 56. https://doi.org/10.1016/j.molliq.2015.12.002.
775 Zeng, Qiang, Yongji Huang, Leiming Huang, Liang Hu, Daoling Xiong, Hui Zhong, and Zhiguo He.
776 2020. “Efficient Removal of Hexavalent Chromium in a Wide PH Range by Composite of
777 SiO2 Supported Nano Ferrous Oxalate.” *Chemical Engineering Journal* 383
778 (March):123209. https://doi.org/10.1016/j.cej.2019.123209.
779 Zhang, Yangyang, Yuanyuan Luo, Xuetao Guo, Tianjiao Xia, Tiecheng Wang, Hanzhong Jia, and
780 Lingyan Zhu. 2020a. “Charge Mediated Interaction of Polystyrene Nanoplastic (PSNP) with
781 Minerals in Aqueous Phase.” *Water Research* 178 (July):115861.
782 https://doi.org/10.1016/j.watres.2020.115861.
783 ———. 2020b. “Charge Mediated Interaction of Polystyrene Nanoplastic (PSNP) with Minerals in
784 Aqueous Phase.” *Water Research* 178 (July):115861.
785 https://doi.org/10.1016/j.watres.2020.115861.
786 Zheng, Ruyi, Timothy C. Germann, Michael Gross, and Mohamed Mehana. 2024. “Molecular
787 Insights into the Impact of Surface Chemistry and Pressure on Quartz Wettability:
788 Resolving Discrepancies for Hydrogen Geo-Storage.” *ACS Sustainable Chemistry &*
789 *Engineering* 12 (14): 5555–63. https://doi.org/10.1021/acssuschemeng.3c08241.
790 Zhou, Fang, Qi Liu, Xu Liu, Wanchun Li, Jian Feng, and Ru-an Chi. 2020. “Surface Electrical
791 Behaviors of Apatite, Dolomite, Quartz, and Phosphate Ore.” *Frontiers in Materials* 7
792 (February):35. https://doi.org/10.3389/fmats.2020.00035.
793 Zhu, Peixin, Yoshitake Masuda, Tetsu Yonezawa, and Kunihito Koumoto. 2003. “Investigation of
794 Apatite Deposition onto Charged Surfaces in Aqueous Solutions Using a Quartz-Crystal
795 Microbalance.” *Journal of the American Ceramic Society* 86 (5): 782–90.
796 https://doi.org/10.1111/j.1151-2916.2003.tb03375.x.
797 Zhuang, Jie, and Gui-Rui Yu. 2002. “Effects of Surface Coatings on Electrochemical Properties
798 and Contaminant Sorption of Clay Minerals.” *Chemosphere* 49 (6): 619–28.
799 https://doi.org/10.1016/S0045-6535(02)00332-6.
800